Extended abstracts from the SME journal
Mining, Metallurgy & Exploration

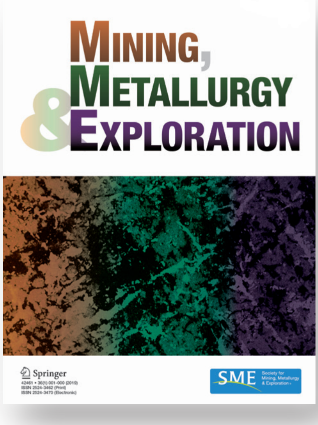

Take full advantage of your SME membership. As a member, you can read and download for free all of the full-text papers in *Mining, Metallurgy & Exploration* (**MME**) and the archives of *Minerals & Metallurgical Processing* (**MMP**). Log in to the SME website as a member, and enter the MME Springer website through our dedicated SME link:

1. Log in at smenet.org with your email address and password.
2. Click on "Publications" in the top banner and choose "Mining, Metallurgy & Exploration journal" in the pull-down menu.
3. Scroll down and click on the "Read the MME Journal Online" link. This takes you to the MME Springer website as an SME member with free access.

To see a specific paper, use the search function or the paper's https://doi link.

For assistance anytime, email Chee Theng at theng@smenet.org. ■

IMPACT FACTOR 2.0

Submit your paper by clicking on the "Submit manuscript" box at springer.com/42461
Get Table of Contents (ToC) email alerts by clicking on "Sign up for alerts"

MME is abstracted and indexed in Web of Science, Current Contents, Science Citation Index Expanded, Scopus, Google Scholar, EBSCO, ProQuest and more.

Invited Extended Abstracts

Collection on Sustainable Development in the Minerals Industry

Advances in mineral processing of hard-rock lithium ores: A comprehensive review

Evaggelos Petrakis, Ilias Alexopoulos, Olga Pantelaki, Vasiliki Karmali and Konstantinos Komnitsas*
School of Mineral Resources Engineering, Technical University of Crete, Chania, Greece
*Corresponding author email: kkomnitsas@tuc.gr

Full-text paper:
Mining, Metallurgy & Exploration (2025) 42:1251–1283, https://doi.org/10.1007/s42461-025-01227-y

Keywords: Pegmatites, Spodumene, Petalite, Flotation, Life cycle analysis, Social license to operate

Lithium (Li) is known as the energy metal of the 21st century due to its use in rechargeable lithium-ion batteries and electronic devices. Its global demand is anticipated to increase from around 700 kt in 2022 to more than 3 Mt in 2030. Today, most lithium is produced from brines; however, its extraction from higher-grade hard-rock deposits attracts noticeable interest. Lithium ore processing faces several challenges, mainly related to environmental impacts and energy consumption. Life cycle assessment (LCA) is an approach that can be used for the quantification of greenhouse-gas (GHG) emissions and energy demand associated with lithium production. Also, the acquirement of social license to operate (SLO) by the mining industry will enable the implementation of exploration and mining projects related to lithium and other energy transition metals, several of which are located near indigenous people's land and environmentally sensitive areas.

Background

Global lithium consumption has been showing a clearly increasing trend over the past 10 years, and in 2023 increased by 27 percent to 180 kt, compared to 2022 data (142 kt) (Fig. 1). The constantly growing demand for lithium-ion batteries (LIBs) has increased the percentage of lithium consumption in the battery sector from 29 percent in 2013 to 87 percent in 2023. Also, the recent rise in lithium demand led to an increase in the number of lithium operations worldwide, with Australia and Chile being the largest lithium producers, accounting for 70 percent of the worldwide output. The global distribution of lithium reserves and production are shown in Table 1. Currently, lithium brines are extracted predominantly in Chile (Atacama deposit) and Argentina (Hombre Muerto deposit), while in Australia Greenbushes is the largest known hard-rock lithium deposit (0.7 Mt). Pegmatite deposits with a typical grade of 1.5 to 4 weight percent lithium oxide (Li_2O) constitute around 25 percent of global estimated reserves. Although several lithium minerals are found in pegmatites, only a few of them, including spodumene (8.1 percent Li_2O), lepidolite (5.9 percent Li_2O) and petalite (4.9 percent Li_2O), have commercial value.

Over the last few years, industry and academia have intensified their efforts to produce high-grade Li concentrates from hard-rock deposits. Typically, mineral processing of hard-rock lithium ores includes comminution for mineral liberation followed by a combination of dense media separation (DMS), magnetic separation and froth flotation. LCA identifies the stages that contribute most to environmental impacts for each major impact category: for example, acidification potential (AP), eutrophication potential (EP), global-warming potential (GWP), land use (LU) and cumulative energy demand (CED).

Table 1 — Global lithium reserves and production by country.

Country	Mine production (metric tons)	Share (percent)	Reserves (metric tons)	Share (percent)
United States*	–	–	1,100,000	4.0
Australia	86,000	46.6	6,200,000	22.4
Chile	44,000	23.8	9,300,000	33.6
China	33,000	17.9	3,000,000	10.8
Argentina	9,600	5.2	3,600,000	13.0
Brazil	4,900	2.7	390,000	1.4
Canada	3,400	1.8	930,000	3.4
Zimbabwe	3,400	1.8	310,000	1.1
Portugal	380	0.2	60,000	0.2
Others	–	–	2,800,000	10.1
Total	184,680	100.0	27,690,000	100.0

*Mine production data not available.

Results and discussion

DMS is mainly used for the coarse separation of lithium-bearing minerals from gangue silicates, such as quartz, feldspars and micas. It is applied in preconcentration stages, so that the downstream processes become more efficient and consume less energy, water and chemical reagents. The biggest challenge in the use of DMS is the small difference in specific gravities among lithium-bearing minerals and gangue silicates (2.55 to 2.80) or iron-bearing silicate minerals, such as amphiboles (2.9 to 3.6) and pyroxenes (3.0 to 4.0). Magnetic separation is usually applied for the removal of iron-bearing gangue minerals, such as amphibole and tourmaline, that cannot be achieved by DMS and flotation. It can be applied prior to DMS or flotation and/or following flotation to produce final concentrates. Froth flotation is particularly used for the treatment of fine particles, having little difference in specific gravities between valuable and gangue minerals. The beneficiation of Li-bearing minerals present in pegmatites can be accomplished by either direct or reverse flotation. Typically, direct flotation is carried out using anionic collectors to float Li-bearing minerals, whereas in the reverse route cationic collectors are employed to float gangue minerals. In addition, due to the very similar points of zero charge (PZC) between lithium-bearing and gangue minerals and the weak adsorption mechanisms prevailing in cationic flotation, the use of selective anionic collectors is necessary. However, in recent years efforts have been made to fully understand the adsorption mechanisms in cases when a combination of anionic/cationic collectors is used. This may potentially lead to increased separation efficiency due to improved selectivity and adsorption capacity.

Table 2 provides data on GWP in kg CO_2-eq/kg Li_2CO_3, obtained from several LCA studies carried out for the processing of Li ores. The different values are due to the treatment of various Li sources as well as the different boundaries used in each study. Therefore, standardization of the LCA methodology is needed to enable a reliable comparison of results for the various impact categories and identification of hotspots.

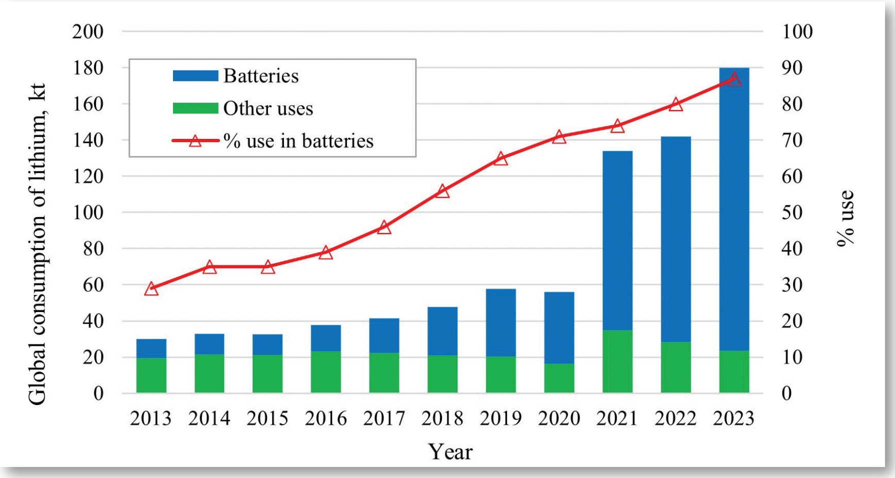

Fig. 1 Global lithium consumption and percentage use, period 2013–2023.

Conclusion

This paper presents the main technologies used for the beneficiation of lithium hard-rock deposits. Emphasis is placed on recent advances and areas that require further research toward the more sustainable and cost-efficient processing of lithium ores.

The quantification of environmental impacts in the entire lithium value chain will increase industry's transparency, eliminate concerns associated with the production of energy transition metals that are needed to tackle climate change, and improve trust between the mining industry and all interested stakeholders, thus increasing the probability that the mining projects will acquire social acceptance. ■

Funding

This study received funding in the frame of LITHOS Horizon Europe (HE) project, "Cost-effective processing and refining of lithium into lithium hydroxide from strategic European multi-mineral lithium hard-rock projects," https://lithos-horizon.eu/, from the European Union's Framework Programme for Research and Innovation Horizon Europe under Grand Agreement Innovation Action No. 101138112.

References

A list of all references is available in the full paper.

Table 2 Global-warming potential (GWP) values (in kg CO_2-eq/kg Li_2CO_3), obtained from various LCA studies.*

GWP (kg CO_2-eq/kg Li_2CO_3)	Source (hard rocks/brines)
5.0 to 25.0	Brine
17.1 to 22.3	Spodumene
5.82	Brines
34	Spodumene (Greenbushes Australia)
14	Spodumene (Mt. Cattlin – Australia)
4	Brines (Salar-de Atacama, Chile)
21.5	Hectorite (Sonora, Mexico)
23.5	Zinnwaldite (Zinnwald, Germany)
15.60	Rock-based lithium
0.329	Brine-based lithium
3.4-8	Various brine deposits
10.7-20.4	Pegmatites
23.4	Spodumene
8.9-16.6	Clays (US)
12-12.6	Low-Li-content brines (LLCBs)

*References to these studies are available in the full paper.

Estimation of uniaxial strength of rock: A comparison between Bayesian-optimized machine learning models

Jitendra Khatti* and Kamaldeep Singh Grover

Department of Civil Engineering, Rajasthan Technical University, Kota, Rajasthan, India

*Corresponding author email: jitendrakhatti197@gmail.com

Full-text paper:

Mining, Metallurgy & Exploration (2025) 42:133–154, https://doi.org/10.1007/s42461-024-01168-y

Keywords: Data simulation, Young's modulus, Multicollinearity, Uniaxial compressive strength

The uniaxial compressive strength (UCS) of rock measures its ability to resist compressive forces under unconfined loading. The laboratory determination of UCS is more time-consuming than the empirical and machine learning (ML) approaches. This investigation employs and compares the different ML approaches to estimate the UCS of rocks. Several statistical analyses introduce the Bayesian-optimized Gaussian process regression (GPR) as the most robust and reliable ML approach that estimates the UCS of rock with a confidence interval of ±75 MPa.

Background

The creep, permeability, porosity, fracture toughness, brittleness, ductility, hardness, Poisson's ratio, Young's modulus and strength (shear, tensile, uniaxial) properties demonstrate the behavior of rocks. The UCS, the most popular mechanical property, presents rock characteristics influenced by the formation process [1]. The UCS of rock is determined by laboratory testing, point load test, Schmidt hammer test, ultrasonic velocity and empirical methods. These methods are more lengthy and time-consuming than the ML approaches [2]. In recent years, the conventional and optimized models of random forest, artificial neural network, adaptive neuro-fuzzy inference system, extreme learning machine and extreme gradient boosting approaches have been utilized to estimate the UCS of rock [3]. The ML approaches are data-driven, and the prediction capabilities of approaches are significantly affected by the quality and quantity of the database [4]. The performance metrics, regression error characteristics (REC) curve, score analysis, uncertainty analysis, convergence and accuracy matrix ensure the prediction capabilities of the ML approaches.

Methodology

This investigation develops the Bayesian-optimized ensemble trees (ET), decision tree (DT), GPR and sup-

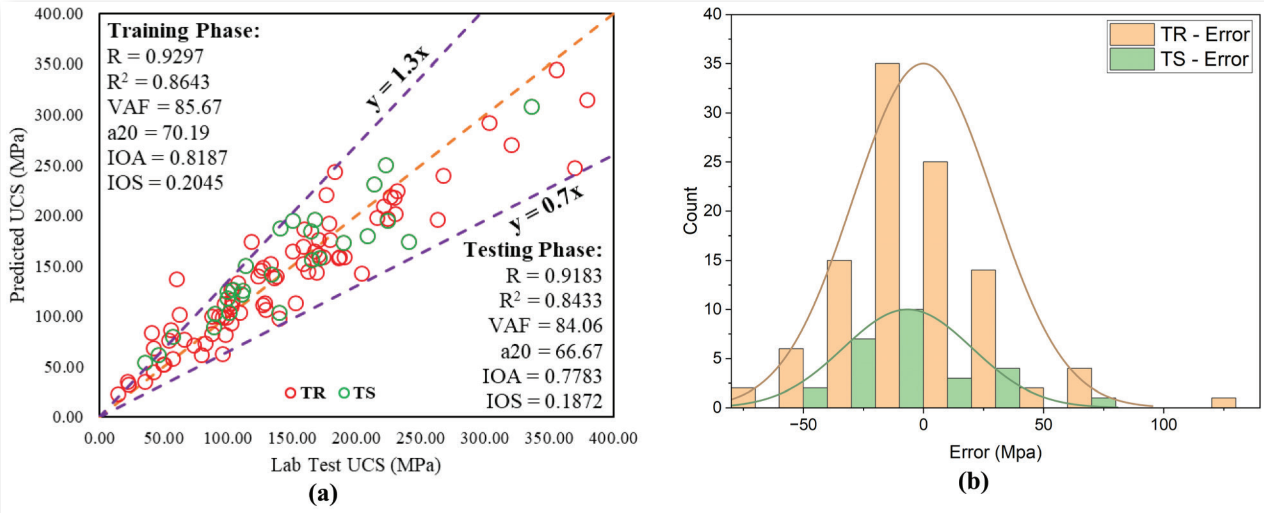

Fig. 1 Illustration of (a) relationship between actual and estimated rock UCS and (b) error distribution plot.

port vector machine (SVM) models to estimate the UCS of rocks. Further, it compares them with the multilinear regression (MLR) model. To develop the models and estimate the UCS of rocks, the P-wave velocity, Young's modulus, density, mass and area properties of 131 rock specimens were utilized as features. The quality and reliability of the database were analyzed using variance analysis (ANOVA), Pearson's product-moment correlation coefficient, multicollinearity and sensitivity analysis. The SVM, GPR, ET and DT models were developed, trained and tested using MATLAB R2020a. Thirteen metrics, including root mean square error (RMSE), mean absolute error (MAE) and performance index (PI), measured and analyzed each ML model. Based on comparing performance metrics, accuracy matrix, REC curve, uncertainty analysis and score analysis, the most reliable ML model was introduced to estimate the UCS of rock.

Results

This investigation trained and tested each ML model using 104 and 27 rock specimens, respectively The performance comparison demonstrated that the GPR model achieved highest performance (R) in training (= 0.9297) and testing (= 0.9183) phase, followed by the ET, MLR, DT and SVM models (Fig. 1). The PI (training = 1.65, testing = 1.62), RMSE (training = 29.1618 MPa, testing = 27.1664 MPa) and MAE (training = 21.8895 MPa, testing = 23.2977 MPa) metrics also demonstrated the significant prediction capabilities of the GPR model because of its ability to model complex, nonlinear relationships with uncertainty quantification. The score analysis (Fig. 2), REC curve (area over the curve 4.51E-03 in training and 3.80E-03 in testing phase), and uncertainty (less uncertainty bandwidth) analysis presented the reliability and robustness of the GPR model over the ET, MLR, DT and SVM models due to its probabilistic predictions with confidence intervals and adapts well to small data sets. Its kernel-based approach enables capturing intricate spatial correlations, making it highly flexible and accurate.

Discussion

This study employed and analyzed the GPR, SVM, DT, ET and MLR models to identify the reliable robust ML model to estimate the UCS of rock. The multicollinearity

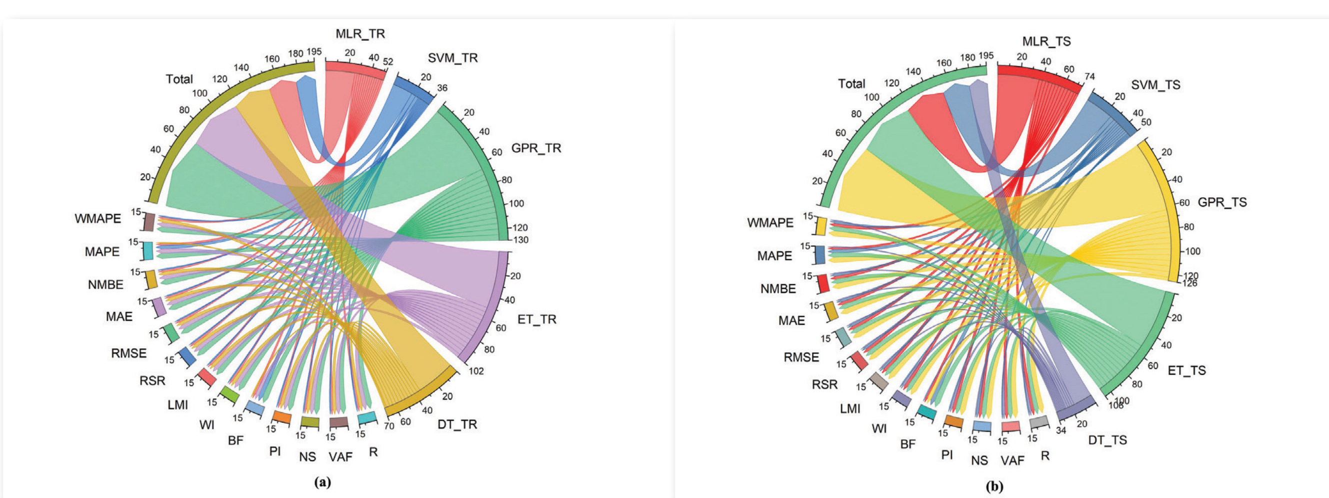

Fig. 2 Illustration of the score analysis of each model in (a) training and (b) testing phase.

parameter — that is, variance inflation factor (VIF) — demonstrated the effect of feature collinearity on the performance and accuracy of te SVM, DT, ET and MLR models in both phases, demonstrated in the convergence plot (Fig. 3). Moreover, the reliability of the GPR model was calculated by implementing a20, index of scatter (IOS) and index of agreement (IOA). It was observed that the GPR estimated rock UCS with a20 (training = 70.19, testing = 66.67), IOA (training = 0.8187, testing = 0.7783) and IOS (training = 0.2045, testing = 0.1872), which are close to the ideal values. In addition, the curve fitting was analyzed by computing the test to train RMSE ratio. It was observed that feature multicollinearity overfitted the MLR (= 1.1213), SVM (= 1.1113), ET (= 1.0950) and DT (1.1900) models. On the other hand, the GPR model predicted the UCS of rock with underfitting: that is, 0.9316 ≈ 1.00. Finally, the GPR model was identified as a robust reliability ML model to estimate the rock UCS.

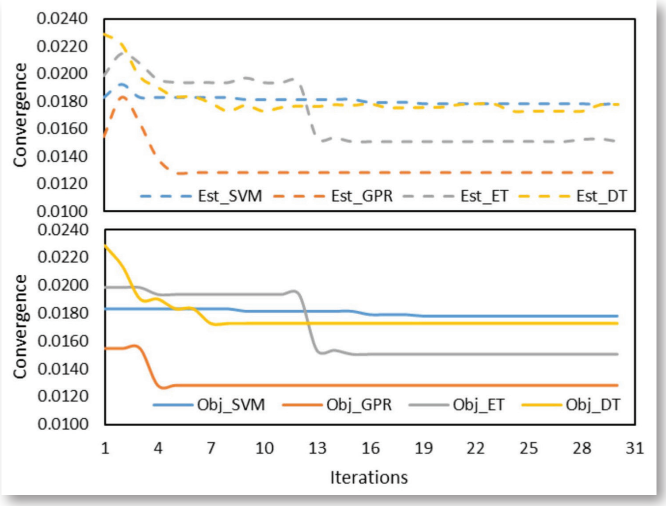

Fig. 3 Illustration of convergence plot for each model in estimating rock UCS.

Conclusions

This study presents an optimal ML model for predicting rock's uniaxial compressive strength (UCS) using five methods: MLR, GPR, SVM, DT and ET. The GPR model outperformed the others, achieving high accuracy and minimal residuals, followed by ET. The study also highlighted the positive influence of specimen area and Young's modulus on GPR and ET performance. At the same time, MLR, SVM and DT performed poorly when these variables showed low sensitivity. Additionally, problematic multicollinearity adversely affected MLR, SVM and DT model accuracy. Future studies may explore other models like LSSVM, GEP and ELM for improved accuracy. ■

Selected references

1. Wang H, Zhang C, Zhou B, Xue S, Jia P, Zhu X (2023) Prediction of triaxial mechanical properties of rocks based on mesoscopic finite element numerical simulation and multi-objective machine learning. J King Saud Univ-Sci. 35(7):102846
2. Chen S, Zhang H, Wang L, Yuan C, Meng X, Yang G, Shen Y, Lu Y (2022) Experimental study on the impact disturbance damage of weakly cemented rock based on fractal characteristics and energy dissipation regulation. Theoret Appl Fract Mech 122:103665
3. Suo Y, Zhao Y, Fu X, He W, Pan Z (2023) Acoustic and mechanical tests of sandstone-shale composites in Songliao Basin and prediction of uniaxial compressive strength. Geoenergy Sci Eng 228:212034
4. Rezaei M, Asadizadeh M (2020) Predicting unconfined compressive strength of intact rock using new hybrid intelligent models. J Mining Environ 11(1):231–246

Fracture initiation pressure as a measure of cemented paste backfill strength

James A. Frimpong[1], Basel Ahmad Shabab[1], Rohit Pandey[1,*], Snehamoy Chatterjee[2], Gabriel Walton[3] and Alexander S. Brand[4]

[1]Mining and Minerals Engineering, Virginia Tech, Blacksburg, VA, USA
[2]Geological and Mining Engineering and Sciences, Michigan Technological University, Houghton, MI, USA
[3]Geology and Geological Engineering, Colorado School of Mines, Golden, CO, USA
[4]Civil and Environmental Engineering, Virginia Tech, Blacksburg, VA, USA
*Corresponding author email: rpandey@vt.edu

Full-text paper:
Mining, Metallurgy & Exploration (2025) 42:1305–1323, https://doi.org/10.1007/s42461-025-01257-6

Keywords: Cemented paste backfill, Fracture initiation pressure, Tensile strength prediction, Failure models

A laboratory-scale hydraulic fracturing method measuring fracture initiation pressure (FIP) is demonstrated as a rapid, high-resolution technique to directly assess the strength of cemented paste backfill (CPB). The approach correlates linearly with conventional CPB strength measurements and is suitable for direct, in situ assessment, empowering mine operators with more reliable and timely quality assurance for underground support.

Background

As underground mining advances to greater depths and processes larger orebodies, responsible tailings management and ground support grow in importance. Cemented paste backfill (CPB) created from mine tailings and cementitious binders, is now widely used to fill mined-out voids, providing ground stability and minimizing environmental impact. Reliable assessment of CPB strength, especially tensile strength, is critical for safe mine design and operational sequencing and to reduce risks of backfill or bulkhead failure.

Current practices typically rely on uniaxial compressive strength (UCS) tests of laboratory-cast cylinders, which are poor proxies for in situ CPB strength due to discrepancies in placement, curing and testing conditions. In situ methods such as coring or penetration tests are time-consuming, challenging and often unsuccessful for low-strength materials. Electrical-conductivity-based monitoring provides indirect assessments but require prior instrumentation. This study addresses the industry's need for a direct, deployable method to assess both early- and late-stage CPB strength with improved reliability.

Methods

A laboratory-scale hydraulic fracturing protocol was developed to determine the FIP of cemented past backfill. CPB samples were prepared from silica tailings and type I Portland cement at three binder dosages (4 percent, 8 percent and 12 percent) and tested after curing for 3, 7, 14 and 28 days. For each condition, standardized UCS, Brazilian tensile strength (BTS) and Mode-I fracture toughness (K_{Ic}) measurements were also performed for benchmarking. The experimental procedure followed for the work presented here is shown in Fig. 1.

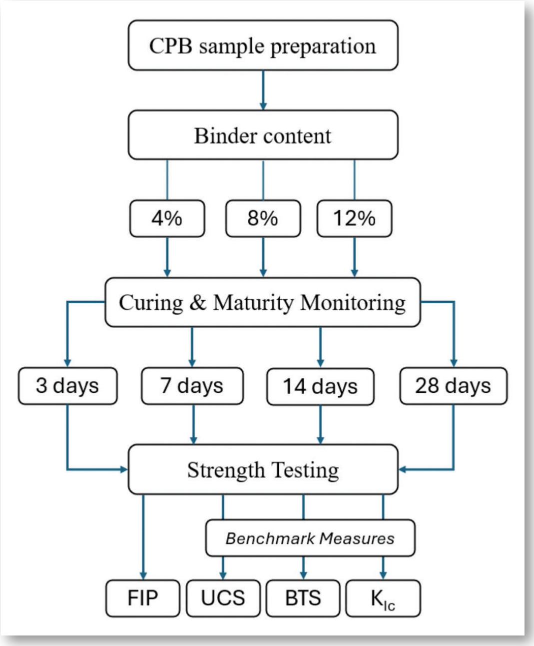

Fig. 1 Experimental plan followed in the research.

To measure FIP, a 2 in. × 4 in. CPB cylinder was prepared with a central borehole (1/8-in. diameter), into which hydraulic oil was injected at a constant flow rate of 4 mL/min. The injection of the hydraulic oil resulted in increase in pressure until a maximum pressure was reached. At the maximum pressure — that is, the FIP — a tensile failure was initiated, thereby providing a direct measure of tensile strength. All tests were conducted in triplicate for reliability.

Results

Figure 2 demonstrates representative hydraulic injection pressure-time curves for CPB samples at varying binder contents and curing durations. In all cases, hydraulic pressure increases gradually under constant oil injection until the FIP is reached. The onset of FIP is consistently delayed and occurs at a lower pressure for low-binder or early-age samples, while higher binder content or extended curing yields markedly higher, earlier peaks.

Quantitative results for all test conditions are summarized in Table 1. Here the mean FIP values are presented alongside UCS, BTS and K_{Ic}. All strength measures exhibit system growth with increased binder and curing duration. Across the data set, FIP is strongly and linearly correlated with all benchmark strength metrics regardless of binder or cure period. On average, FIP is approximately 1.6 times the UCS, 6.6 times the BTS and 10.1 times the K_{Ic}. The higher resolution of FIP as a measure of strength compared to other measures is attributed to the borehole size dependence of FIP as a measure of strength, as described by the point stress mode, which is discussed later.

Together, Fig. 2 and Table 1 illustrate that FIP is a robust, sensitive measure of CPB strength, with clear evolution across binder and maturity conditions and strong predictive value with respect to established mechanical benchmarks.

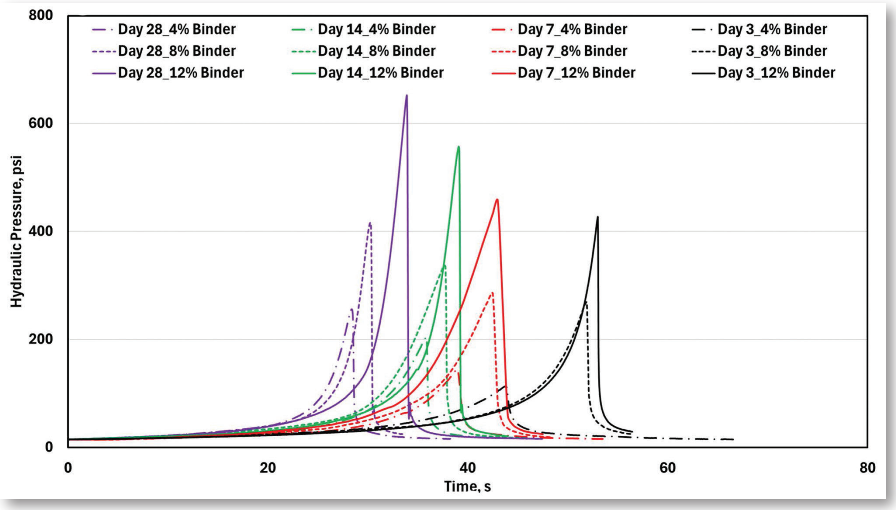

Fig. 2 Hydraulic injection pressures obtained during fracturing of CPB samples at various binder contents and cure periods.

Discussion

Hydraulic fracturing, as validated in this study, offers a breakthrough for real-time, direct assessment of in situ CPB strength, especially for mine sites where sample extraction or prior instrumentation is infeasible. The technique's sensitivity and high resolution at small borehole diameters enable early detection of weak backfill, supporting improved operational decisions, bulkhead management and enhanced mine safety.

The point stress (PS) model explains why FIP can significantly exceed the BTS-derived tensile strength for small borehole diameters. Small borehole diameters decrease the likelihood of sampling a critical flaw, thereby artificially elevating the FIP beyond the tensile strength of the material. Thus, practitioners can leverage small boreholes for sensitivity strength assessment or opt for larger borehole diameters to directly measure the true tensile strength, providing flexibility in application.

While the PS model shows strong agreement with laboratory data, its predictive accuracy may vary with different backfill compositions, binder types and site-specific conditions. Validating and calibrating the approach under true in situ stress environments and at field scale are important next steps to ensure robust operational performance. Additionally, further investigation into how microstructural variables, such as particle size distribution, binder chemistry and hydration mechanisms influence the characteristic distance in the PS model will help refine its applicability and support broader adoption across a range of underground mining scenarios.

Table 1 — Mean and standard deviation (within parentheses) values of the measures of benchmark strength measures and FIP for CPB.

Day	Binder (percent)	UCS (psi)	BTS (psi)	K_{Ic} (psi√in)	FIP (psi)
3	4	51.4 (±3.2)	9.4 (±0.4)	9.3 (±1.9)	117.6 (±37.8)
	8	110.0 (±4.6)	30.3 (±3.5)	22.8 (±2.6)	261.0 (±27.4)
	12	248.9 (±5.2)	59.8 (±5.0)	39.4 (±2.3)	411.7 (±66.6)
7	4	60.4 (±3.4)	15.4 (±2.4)	16.7 (±2.6)	142.4 (±21.3)
	8	135.6 (±8.3)	38.9 (±4.1)	28.5 (±2.8)	264.8 (±28.5)
	12	283.6 (±16.5)	71.8 (±9.5)	42.0 (±0.4)	444.1 (±39.7)
14	4	85.3 (±6.2)	18.8 (±4.1)	18.8 (±0.7)	205.7 (±12.8)
	8	184.2 (±12.1)	44.8 (±2.7)	36.2 (±3.0)	338.3 (±11.5)
	12	385.3 (±3.8)	81.2 (±18.2)	58.2 (±2.1)	565.8 (±54.8)
28	4	120.0 (±6.2)	27.1 (±4.6)	18.7 (±0.3)	250.5 (±34.1)
	8	245.6 (±14.0)	54.9 (±17.6)	42.6 (±2.1)	415.1 (±1.5)
	12	493.6 (±10.8)	119.4 (±19.2)	69.5 (±1.4)	639.3 (±27.6)

Conclusions

- Hydraulic fracturing (FIP measurement) is a validated, direct method for CPB strength assessment, correlating with established benchmarks.
- The size-dependent point stress model enables practical field use and interprets FIP-benchmark relations accurately.
- This method supports rapid, in situ strength verification, improving operational safety and efficiency in underground mining. ■

References

A list of all references is available in the full paper.

YOLO-based miner detection using thermal images in underground mines

Cyrus Addy[1,*], Venkata Sriram Siddhardh Nadendla[2] and Kwame Awuah-Offei[1]

[1]Department of Mining and Explosives Engineering, Missouri University of Science and Technology, Rolla, MO, USA

[2]Department of Computer Science, Missouri University of Science and Technology, MO, USA

*Corresponding author email: ca8mc@mst.edu

Full-text paper:
Mining, Metallurgy & Exploration (2025) 42:1369–1386, https://doi.org/10.1007/s42461-025-01249-6

Keywords: Object detection, Miner detection, Thermal image, YOLO, Underground mine

Mine emergencies result in fatalities that can be reduced by using well-designed and effective in-mine robots. In-mine robots can be used for many tasks, such as structural monitoring, environmental surveillance and payload delivery. As no robots currently detect miners in real time in underground low-light conditions, we investigate challenges in applying object detection algorithms using thermal images. Our team generated a unique data set at the Missouri University of Science and Technology Experimental Mine using a FLIR TG297 thermal camera, dividing it into 450 training and 50 validation images. Using 10-fold cross-validation, we trained the You Only Look Once version 5 (YOLOv5) and You Only Look Once version 8 (YOLOv8) algorithms via transfer learning for 50 epochs. The retrained YOLOv8 outperformed the retrained YOLOv5 on the validation data set. In a simulated mine fire emergency, both models showed significant improvement, with YOLOv8n's mAP rising from 13.90 percent to 74.70 percent and YOLOv5n's from 42.10 percent to 68.30 percent after transfer learning.

Introduction

Robots have a huge role to play in mine emergency response. Although robot developers have incorporated various sensors to facilitate operator vision, decoding sensor feeds in low-light conditions remains challenging, and robots need autonomous object detection capabilities for missions without livestreamed video. This requires advanced intelligent robot vision.

Advanced object detection algorithms make it possible to intelligently detect miners for quick evacuation decisions during underground mine emergencies. Researchers train state-of-the-art object detection algorithms using image data sets to predict outcomes accurately. However, while there are large data sets for training such algorithms in other contexts, the reverse is true for underground miner detection due to security and privacy concerns. This study addresses these gaps by generating a unique thermal image data set for underground miner detection, employing transfer learning to develop models for real-time miner detection, and testing these models in a practical emergency scenario.

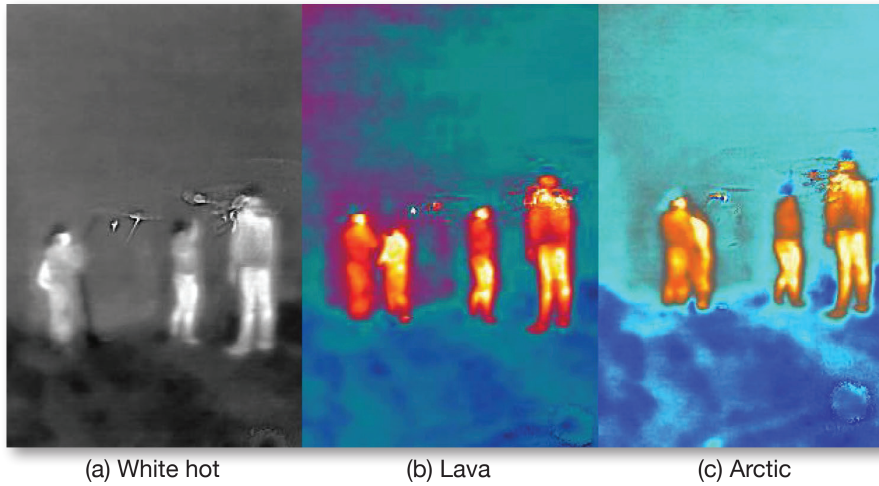

Fig. 1 Color palette of the captured images.

Method

This study employed three main methods: (1) data collection and labeling, (2) data processing and (3) experimentation. We collected image data at the Missouri University of Science and Technology Experimental Mine, which is an underground room-and-pillar limestone mine.

The approximately 500 images, collected using a FLIR TG297 handheld camera, captured miners engaging in marking out, drilling and blasting. Figure 1 shows the color palette of the captured images.

We performed experiments on a Dell workstation, using the pretrained weights for different variants of the two models. For the experiments, we used 50 epochs (starting from 5, with increments of 5), a batch size of 10, an AdamW optimizer, initial and final learning rates of 0.01, and four classes. After the experiments, the best weight files of the best-performing models were used for inference in a simulated fire scenario. The metrics of evaluation were mean average precision (mAP), precision, recall and F1 score, all captured within a scale of 0 to 1 (0 for poor, and 1 for excellent).

Results and discussion

We used the transfer-learned models to detect miners in selected images to assess their efficacy. The results showed that transfer learning enhanced the models' capacity to identify miners (Fig. 2). The retrained YOLOv5 and YOLOv8 models achieved detection performance using our thermal images that is comparable to RGB images object detection results reported in literature. YOLOv8 significantly improved, with YOLOv8m's mAP increasing from 41.20 percent to 70.20 percent, and YOLOv8n's from 13.90 percent to 74.70 percent, after transfer learning. Similarly, YOLOv5 variants improved significantly, YOLOv5m's mAP increased from 40.60 percent to 66.20 percent and YOLOv5n's from 42.10 percent to 68.30 percent.

To assess the efficacy of the retrained algorithms in fire emergencies, we used the optimal weight file from the 50th epoch of each variant for inference, from the fold with the highest number of person-class instances and the highest mAP_50, on the fire emergency data set. We conducted this inference for five variants of YOLOv5 and YOLOv8 to assess their efficacy in detecting individuals underground during a fire emergency. The findings indicate that meticulously implemented transfer learning, using existing algorithms (YOLOv5 and YOLOv8), can enhance their performance in the simulated fire emergency. Fire-induced shadows caused false detections, and the models struggled to generalize miner features, mistakenly detecting flames as a person in one frame (Fig. 3). The retrained models performed worse in fire than in a normal situation; future studies should expand data sets to cover diverse mine emergencies.

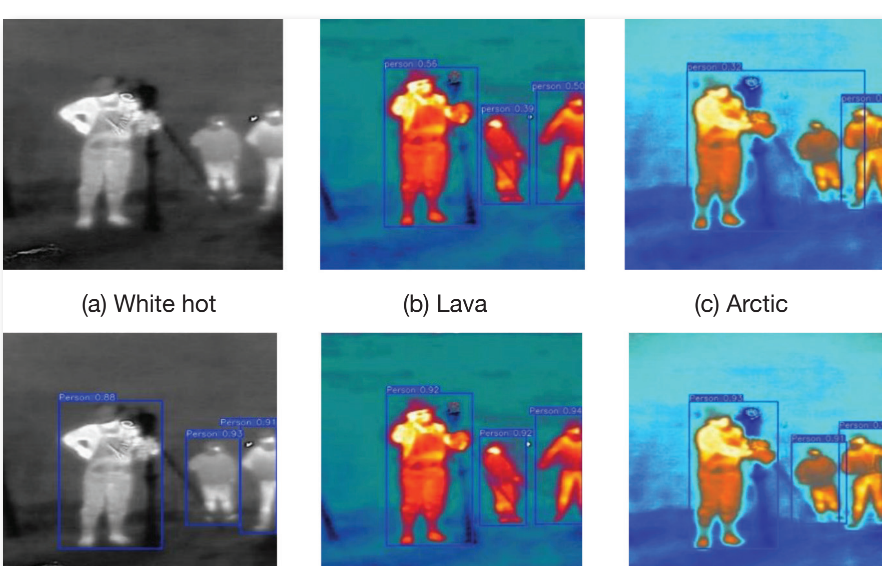

Fig. 2 YOLOv5 detection performance: (top) before transfer learning and (bottom) after transfer learning.

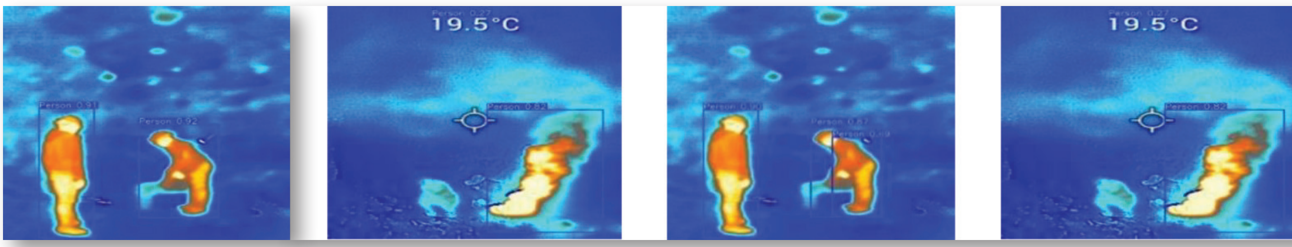

(a) (b)

Fig. 3 Detection using fire images for the nanovariant of both models: (a) using transfer-learned YOLOv5n and (b) using transfer-learned YOLOv8n.

Conclusion

This work used transfer learning to develop object detection models for thermal images in mines using YOLOv5 and YOLOv8 on a preliminary data set of underground miners' thermal images. YOLOv8 proved the best choice for underground robots with thermal cameras, especially given the high stakes of mine emergencies. Inference on simulated fire emergency shows that both models after transfer learning,can detect miners in this "foreign" data set better than the untrained models: YOLOv8n's mAP increased from 13.90 percent to 74.70 percent and YOLOv5n's from 42.10 percent to 68.30 percent. Despite these gains, the retrained algorithms underperformed in the simulated fire emergency. To further improve performance across diverse mine emergencies, we recommend using a larger data set for transfer learning. ■

Funding

This project was funded by the Centers for Disease Control/National Occupational Safety and Health (CDC-NIOSH) contract #U60OH012350 - 01–00.

References

A list of all references is available in the full paper.

Selected Abstract

Effects of stockpiling on topsoil biogeochemistry for semiarid mine reclamation

Jessica Ledesma[1,2], Julia W. Neilson[1], Raina M. Maier[1], Alicja Babst-Kostecka[1] and Craig Rasmussen[1,*]
[1]The Department of Environmental Science, The University of Arizona, Tucson, AZ, USA
[2]Geosystems Analysis Inc., Tucson, AZ, USA
*Corresponding author email: crasmuss@arizona.edu

Full-text paper:
Mining, Metallurgy & Exploration (2025) 42:15–26, https://doi.org/10.1007/s42461-024-01164-2

Keywords: Topsoil stockpile, Copper mining, Mine reclamation, Soil biogeochemistry, Redox processes, Semiarid climate

Stockpiling and storage of topsoil for use in reclamation and revegetation are common practices for many mining operations. However, stockpiling can lead to significant changes in topsoil physical and biogeochemical properties that may be detrimental to reclamation. The objective of this research was to assess the effect of long-term stockpiling on soil biogeochemical properties in a semiarid region. We hypothesized that soil properties would change systematically with depth, reflecting a shift to anaerobic conditions and resulting in a general decrease in soil health. To address this hypothesis, boreholes more than 20-m deep were drilled into a 14-year-old topsoil stockpile at a copper mine in Arizona and samples collected every approximately 75 cm. Samples were analyzed for soil DNA biomass, texture, general agronomic properties, mineral composition, oxalate and dithionite extraction of active mineral phases, and total elemental composition. Depth profiles revealed nonsystematic changes in biogeochemical variables with depth, including variation in soil DNA biomass, organic matter (OM), extractable nitrate (NO_3-N) and ammonium (NH_4-N) nitrogen, plant-available manganese (Mn) and iron (Fe), and oxalate-extractable Mn and Fe. Differences in biogeochemical properties were associated with zones of variable redox state mediated by OM content and layer depth. Anaerobic zones were observed at depths greater than 4 m where OM > 1 percent, and aerobic zones were observed at depths up to 15m where OM < 1 percent. This study demonstrates the importance of stockpile composition on biogeochemical processes during storage and contributes to improved understanding of topsoil management as a resource for reclamation of degraded mine lands in semiarid environments. ■